JOURNAL OF MATERIALS SCIENCE 26 (1991) 951–956

Laser cladding of zirconium on magnesium for improved corrosion properties

R. SUBRAMANIAN, S. SIRCAR, J. MAZUMDER
Laser Aided Materials Processing Laboratory, Department of Mechanical and Industrial Engineering, University of Illinois at Urbana-Champaign, 1206 West Green Street, Urbana, Illinois, USA

Laser cladding of Mg–2 wt% Zr, and Mg–5 wt% Zr powder mixture onto magnesium was carried out. The microstructure of the laser clad was studied. From the microstructural study, the epitaxial regrowth of the clad region on the underlying substrate was observed. Martensite plates of different size were observed in transmission electron microscope for Mg–2 wt% Zr and Mg–5 wt% Zr laser clad. The corrosion properties of the laser clad were evaluated in sea-water (3.5% NaCl). The position of the laser claddings in the galvanic series of metals in sea-water, the anodic polarization characteristics of the laser claddings and the protective nature and the stability of the passivating film formed have been determined. The formation of pitting on the surface of the laser clad subjected to corrosion has been reported. The corrosion properties of the laser claddings have been compared with that of the commercially used magnesium alloy AZ91B.

1. Introduction

Magnesium is one of the prime candidates for structural applications in the aerospace industry where use of a low density material is essential. Magnesium has the lowest density of all engineering materials. A major obstacle to the use of magnesium in structural application is its poor corrosion resistance in wet and salt-laden environments. Magnesium lies at the extreme in the active end of the galvanic series of metals in sea-water. This makes magnesium and its alloys vulnerable to galvanic attack when coupled with more noble metals.

Zirconium was chosen as the alloying element in the present work on a rational basis as described below. Zirconium lies at the noble end of the galvanic series of metals in sea-water. The solid solution of zirconium in magnesium will shift the position of the alloy towards the noble end of the galvanic series of metals in sea-water. Zirconium in salt-laden environments has excellent corrosion resistance.

It has been reported that microstructural refinement due to rapid solidification of magnesium alloys results in improvements in corrosion resistance. Chang *et al.* [1–3] studied the rapid solidification of Mg–Al and Mg–Zn–Al base alloys containing silicon, yttrium or lanthanides. They showed that grain refinement due to rapid solidification resulted in improved corrosion resistance in extruded material compared with the wrought ingot alloys of the ZK60 and AZ91HP type.

The inherent rapid solidification involved in laser material processing results in improved corrosion properties of magnesium alloys [4]. Kattamis [5] have reported on the affect of laser and electron beam surface melting on the microstructure and corrosion behaviour of the wrought magnesium alloy, ZK60 (Mg–6 wt % Zn–0.7 wt % Zr).

Kalimullin *et al.* [6] have reported that laser surface treatment increases substantially the corrosion resistance of the Mg–Li base alloy MA21 (Mg–8 wt % Li–5 wt % Al–4 wt % Cd–1 wt % Zr–0.4 wt % Mn) in 3% NaCl. Irradiation with a CO_2 laser at 40 W mm^{-2} refined the microstructure to a depth of 1.5 mm and raised the corrosion resistance of the alloy. In the laser-affected zone, the alloy has a homogeneous fine-grained microstructure.

The laser cladding technique can be used to improve the corrosion properties of magnesium. The approach to improve the corrosion resistance by laser processing is through the rapid solidification. The inherent rapid solidification involved in laser cladding results in microstructural refinement, extension of solubility limit and formation of non-equilibrium crystalline or amorphous phases. This ultimately results in improved corrosion resistance.

2. Experimental procedure

2.1. Laser cladding

In situ laser cladding of Mg–2 wt % Zr and Mg–5 wt % Zr metal powder mixture was carried out onto the magnesium substrates. The experimental set up consisting of the stainless steel chamber, screw feeder, and gas distribution arrangement used to carry out laser cladding is shown in Fig. 1, schematically. Since magnesium is pyrophoric, the laser cladding was carried out inside the stainless steel chamber. Helium gas was used to provide an inert atmosphere inside the

0022–2461/90 $03.00 + .12

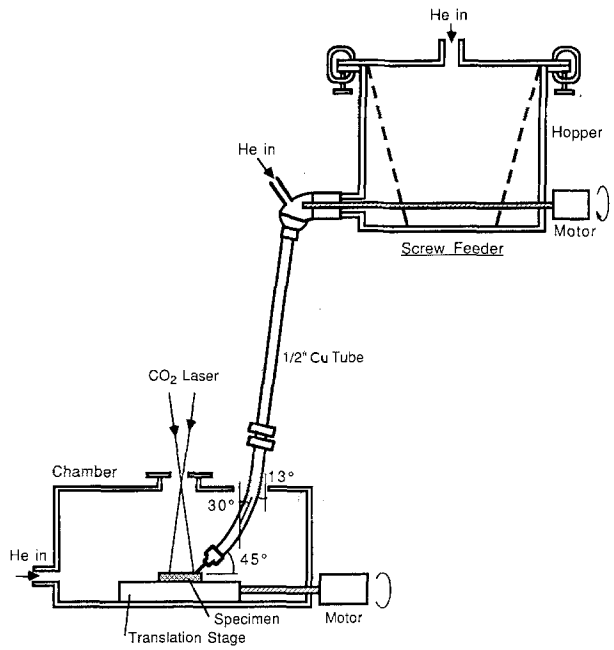

Figure 1 Schematic diagram of the experimental setup used for laser cladding in Mg–Zr system.

TABLE I Laser cladding process parameters

Laser beam power	3 kW
Beam diameter	0.005 m
Beam focus condition	Beam diverges through the substrate
Translation speed	0.00635 m s^{-1}
Shielding gas used	Helium
Powder feed rate	0.355 g s^{-1}

chamber. The helium gas enters into the chamber through the bottom and goes out through the opening in the closing lid on top of the chamber. The translation stage inside the chamber was driven by the stepping motor controlled by the Velmex controller. The powder delivery tube receives the powder from the screw feeder and enters into the chamber through an elliptical hole on the top lid of the chamber. Careful alignment of the laser beam and the nozzle of the powder delivery tube ensured that *in situ* laser cladding conditions were established. Before the alignment, the experimental set up was brought to the working condition. The chamber was positioned under the water cooled copper mirror which deflects the laser beam down on to the substrate kept on the translation stage. The screw feeder was positioned on a steel frame above the chamber. The powder delivery tube was connected to the delivery end of the screw-feeder. The other end of the delivery tube was inserted into the chamber. The shielding gas arrangement is shown in Fig. 1. The gas flow into the hopper of the screwfeeder and the nozzle of the powder delivery tube was controlled by flow meters. Process parameters used for laser cladding are given in Table I.

2.2. Microstructure evaluation

Microstructural investigations of clad specimens were carried out by optical and electron microscopy. Samples for transmission electron microscopy were sectioned from the laser clad region. The top surface of the laser clad was ground to a flat surface using 600 grid emery paper. The low speed diamond saw was used to cut a thin slice from the clad region near the clad–substrate interface. This slice was further thinned (mechanically) to a thickness range of 3 to 5 mm. Discs of 3 mm diameter were punched out from these thin sections. Specimens for TEM observation were prepared by dimpling followed by an Argon ion-beam thinning technique.

2.3. Corrosion testing

The corrosion behaviour of the laser clad was evaluated by using EG&G PARC model 351 corrosion measurement system. This system consists of a model 1000 processor, a model 272 potentiostat, a corrosion cell and a plotter. The corrosion cell set up consists of a glass cell, specimen holder assembly, counter electrodes, bridge tube and saturated calomel electrode. A flat washer limits the area of the corrosion specimen to 1 cm^2 which will be exposed to the electrolyte. Two O-rings prevent leakage of electrolyte into the sample holder so as to eliminate crevice corrosion.

The corrosion specimens from the laser clad were prepared in the following manner. The top surface of the laser clad was ground to a flat surface on 600 grid emery paper. The low speed diamond saw was used to cut a sample of 0.003 m thickness from the laser clad as shown in Fig. 2. From this sample, a disc of 0.015 m diameter was made by cutting with a low speed diamond saw and polishing on 600 grid emery paper to round the corners.

One corrosion cell set up is sufficient to carry out different corrosion tests using a fresh sample and fresh solution for each test. The corrosion cell set up for each test was made as described below. The specimen was immersed in the electrolyte, 3.5 wt % NaCl. The same solution was taken in the bridge tube which acts as the salt bridge. The narrow end of the bridge tube acts as a probe and was fitted with a porous glass tip. The tip, 2 mm in diameter, is a semipermeable membrane. It provides ultra-low liquid leakage rates and minimum IR drop through the tip. The bridge tube was positioned firmly in the corrosion cell using a clip and its position was adjusted to keep the distance between the tip and the surface of the corrosion specimen at 2 mm. The saturated calomel electrode was inserted into the open end of the bridge tube.

The experimental technique of each corrosion test is explained below. In all cases, the experiment was carried out by entering the test parameters in the model 1000 processor in conjunction with the model 272 potentiostat.

2.3.1. Corrosion potential (E_{corr})

As soon as the corrosion specimen is immersed in the electrolyte, the test is initiated through the model 1000 processor. The potential at the surface of the specimen was measured with reference to the saturated calomel electrode as a function of time. The test was run for

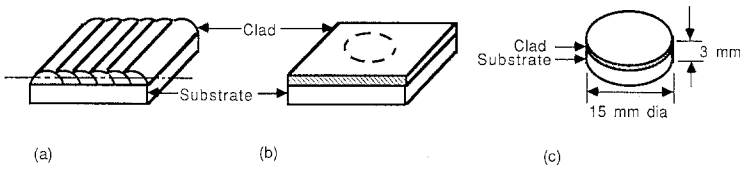

Figure 2 Preparation of corrosion specimen from the clad. (a) Laser clad, (b) surface flattened clad, (c) corrosion sample.

1000 sec and the equilibrium corrosion potential was read from the horizontal portion of the corrosion potential curve. From the corrosion potential measured, the position of the alloy in the galvanic series of metals in sea-water can be determined. The corrosion potential of the alloys in the noble end of the galvanic series will be more positive than that of the alloys in the active end.

2.3.2. Potentiodynamic anodic polarization test

The corrosion specimen was immersed in the electrolyte. The initial delay was set to 1000 sec. As the potential was scanned from a value more negative relative to E_{corr} to a value more positive relative to E_{corr}, the current was measured and plotted as voltage against logarithmic current density. The resulting plot is a potentiodynamic anodic polarization plot. From this plot, the current density at which the passive film forms can be found. The decrease in the current density a_s the potential is scanned in the anodic direction will indicate the change in the surface condition of the sample. Significant decrease in the current density is due to the formation of protective film on the surface.

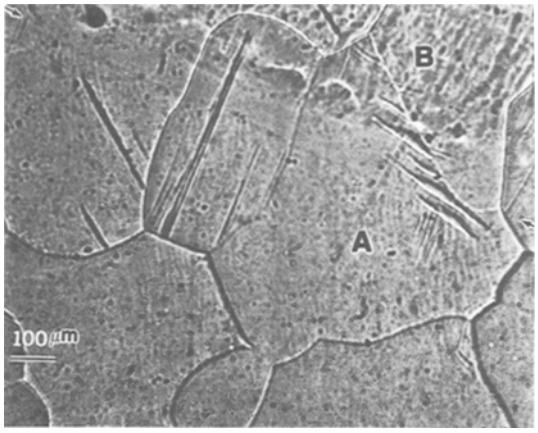

Figure 3 Optical micrograph of the substrate laser clad region. Region A is the substrate and Region B is the cladding.

3. Results and discussion

3.1. Microstructure

The study of the laser clad region in optical microscope shows that homogeneous microstructure was developed. Fig. 3 shows the microstructure of the laser clad. In the microstructure, the substrate is identified as A and the clad region as B. The interface is marked by the arrow. The good fusion between the clad and the substrate can be seen. There are grains common to both the clad and the substrate. This is attributable to epitaxial regrowth of the melt pool on the underlying grain structure of the unmelted substrate.

Lath-type martensitic plates of different size were observed during investigation by electron microscopy in the thin foil prepared from the Mg–5 wt % Zr laser clad. Figs 4a and b show the bright field micrograph of the plates in different regions of the foil. The plates contain substantial dislocations. The composition of the plate shown in Fig. 4b was determined by EDAX. The EDAX spectrum from this plate is shown in Fig. 5. The quantitative analysis of this spectrum shows that the composition of the plate is Mg–2.144 wt % Zr.

The crystal structure of the plate was determined by selected area diffraction. Fig. 6 shows the bright field micrograph of an adjacent region of plates in the foil.

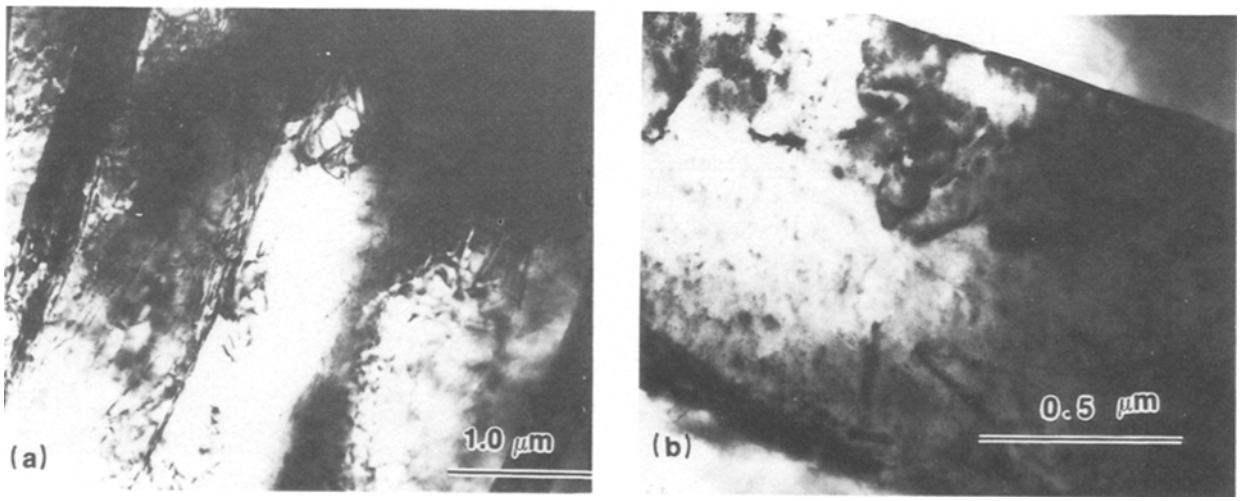

Figure 4 Bright field electron micrographs of the laser clad region.

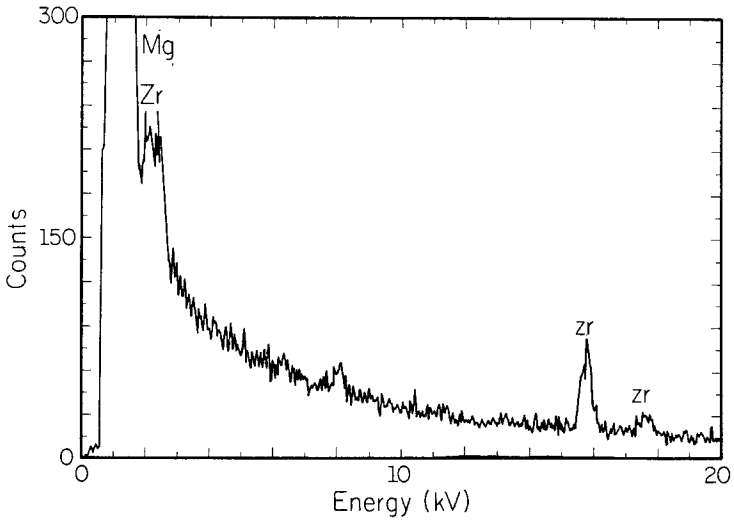

Figure 5 EDAX spectrum obtained from plate like structure in Fig. 4b.

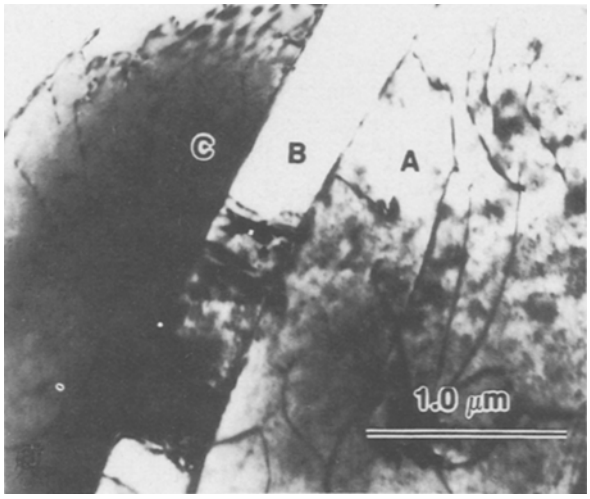

Figure 6 Bright field micrograph of a different region in the foil showing the plate like structures.

Selected area diffraction patterns were recorded from the plate identified as A in Fig. 6. Figs 7a and b show the selected area diffraction patterns of the zones $[2\bar{1}\bar{1}0]$ and $[10\bar{1}1]$ respectively, obtained from this plate A. The c/a ratio of magnesium is 1.623. The c/a ratio calculated from these diffraction patterns is 1.626.

The compositions of these plates were determined using EDAX. The quantitative analysis of these spectra were carried out. The composition of the plate A was found to be Mg–2.711 wt % Zr. The composition of the plate B was found to be Mg–2.46 wt % Zr. The composition of the plate C was found to be Mg–2.46 wt % Zr. The equilibrium solid solubility of zirconium in magnesium is 3.6 wt % Zr. In the present work, in the case of Mg–5 wt % Zr laser clad, it was found that zirconium dissolves in magnesium to an extent of 2.711 wt % under the process conditions given in Table I. The compositions of these plates applies only to that portion of the clad–substrate interface present in the thinned foil.

3.2. Corrosion

The corrosion potential of Mg–2 wt % Zr laser clad was found to be − 1.610 V against SCE as shown in

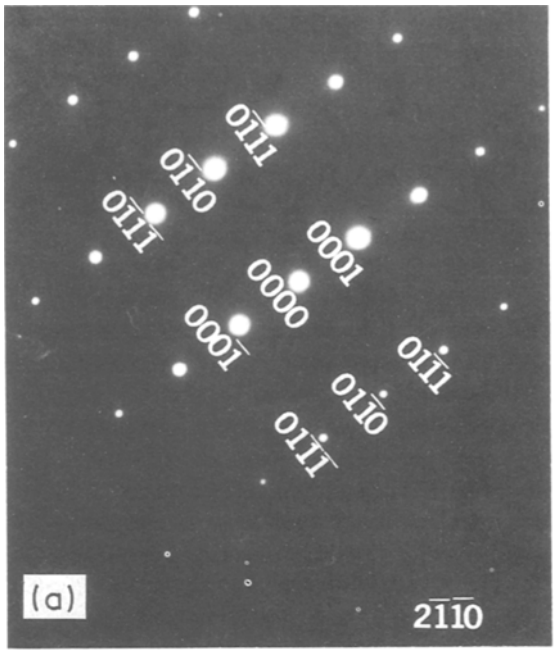

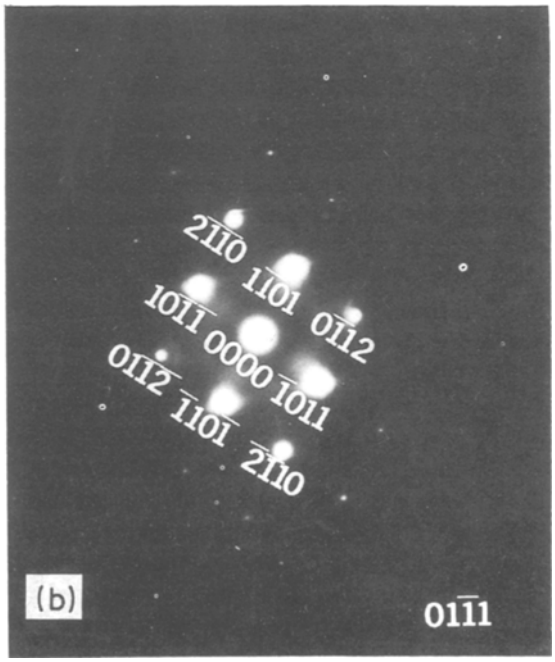

Figure 7 (a) and (b) Selected area diffraction pattern of zone axis $[2\bar{1}\bar{1}0]$ and $[10\bar{1}1]$ respectively obtained from the plate A in Fig. 5.

Fig. 8. The corrosion potential of Mg–5 wt % Zr laser clad has been found to be − 1.57 V against SCE as shown in Fig. 9. The corrosion potential for 100% wt zirconium on magnesium is 0.647 V. The corrosion potential of magnesium in sea-water is − 1.66 V against SCE. It seems that the corrosion potential of the laser claddings becomes more positive with increase in zirconium addition. This shows that addition of zirconium in magnesium shifts the position of the laser clad towards the noble end of the galvanic series of metals in sea water.

The potentiodynamic anodic polarization plots of Mg–2 wt % Zr and Mg–5 wt % Zr laser claddings are shown in Figs 10 and 11, respectively. The incomplete passive film, in the case of both the laser claddings, forms at an anodic current density of 0.398 A cm^{-2}. Subsequent scan in the anodic direction results in the decrease of the current density to a minimum of 0.251 A cm^{-2}. Continued corrosion results in the pitting of the surface. This is in conjunction with the increase in the anodic current density as the potential is scanned further in the anodic direction.

The potentiodynamic anodic polarization plot of the alloy AZ91B is given in Fig. 12. As seen from this plot, it is evident that there is no passive film formation in the case of alloy AZ91B. The anodic current density is 1.32 A cm^{-2} which is much larger than that of the laser claddings. As the potential is scanned in the anodic direction, the current density stays constant at this value and rapid corrosion takes place.

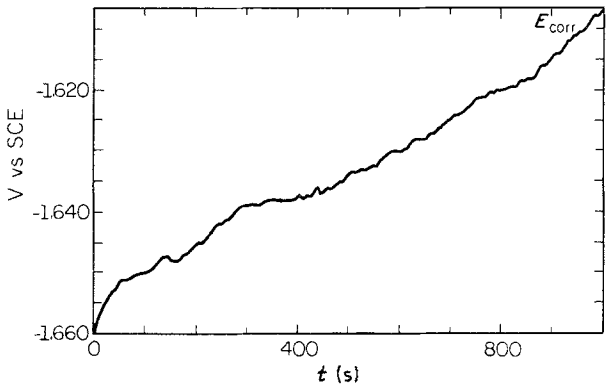

Figure 8 Corrosion potential of Mg–2 wt % Zr clad.

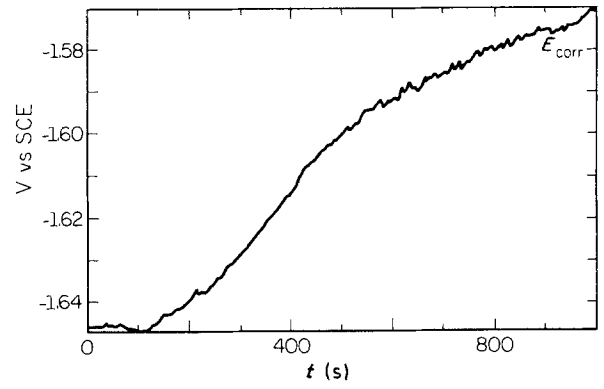

Figure 9 Corrosion potential of Mg–5 wt % Zr clad.

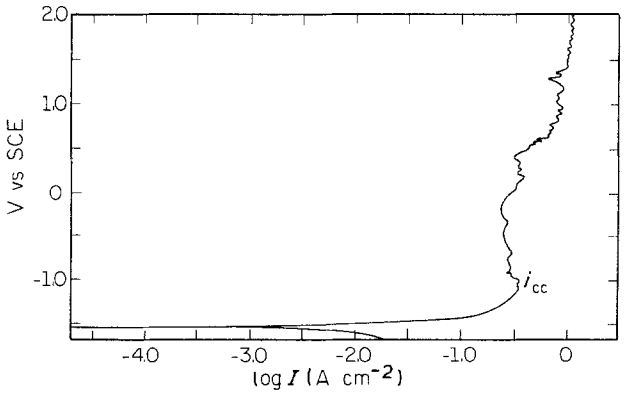

Figure 10 Potentiodynamic anodic polarization curve for Mg–2 wt % Zr clad.

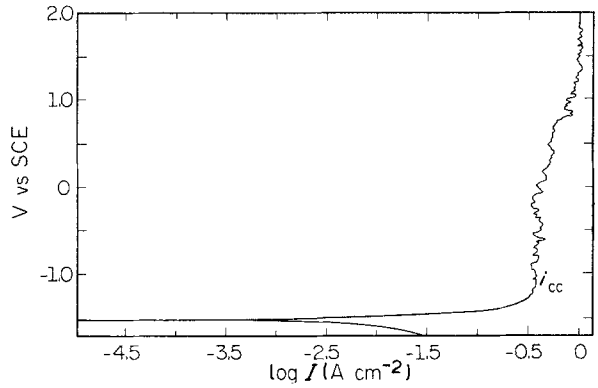

Figure 11 Potentiodynamic anodic polarization curve for Mg–5 wt % Zr clad.

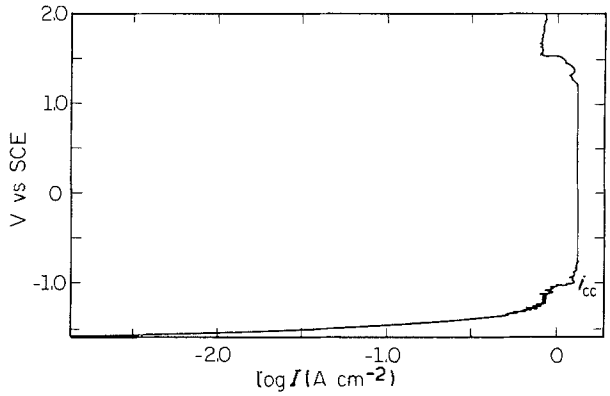

Figure 12 Potentiodynamic anodic polarization curve for Mg alloy, AZ91B.

Addition of zirconium to magnesium seems to improve the resistance to corrosion in 3.5 NaCl solution.

4. Conclusions

The study of the laser clad region in the optical microscope shows the development of homogeneous microstructure. There are grains common to the clad region and the substrate. This could be attributed to the epitaxial regrowth of the melt pool on the microstructure of the unmelted substrate. Electron microscopy revealed mainly h c p martensitic structure for Mg–2 wt % Zr and Mg–5 wt % Zr alloys.

The addition of zirconium to magnesium shifts the alloy towards the noble side in the galvanic series of metals in sea-water. Zirconium forms a passivating film on the surface which prevents further attack by chloride solution. The current density in the passivation region is reduced from 0.398 A cm^{-2} to a minimum of 0.251 A cm^{-2}. It has been found that the laser cladding undergoes pitting type of corrosion in the NaCl solution. This is evident from the study of the surface of the corrosion sample of the laser clad subjected to the potentiodynamic anodic polarization test. The pitting on the surface was observed.

From the potentiodynamic anodic polarization test, it was found that the anodic current density in the passivation region of the laser clad is 0.398 A cm^{-2} which is lower than that of the alloy AZ91B. Subsequent scan in the anodic direction results in the decrease in current density from 0.398 A cm^{-2} to a minimum of 0.251 A cm^{-2}.

Acknowledgement

This work was supported by grants from US Air Force Office of Scientific Research (Grant No. AFOSR 85-0333 and AFOSR 86-0034). Dr Alan Rosenstein is the program manager.

References

1. S. K. DAS and C. F. CHANG, "Rapidly Solidified Crystalline Alloys", edited by S. K. Das *et al.*, (The Metals Society of AIME, Warrendale, PA, 1985) pp. 137–156.
2. C. F. CHANG, S. K. DAS, and D. RAYBOULD, "Rapidly Solidified Materials", edited by P. W. Lee, R. S. Carbonara (American Society for Metals, Metals Park, OH, 1986) pp. 129–135.
3. C. F. CHANG, S. K. DAS, D. RAYBOULD and A. BROWN, *Met. Powd. Rep.* **41** (1986) pp. 302–308.
4. F. HEHMANN and H. JONES, *Proceedings of London Conference* (Institute of Metals, November 1980) pp. 83–96.
5. T. Z. KATTAMIS, in "Lasers in Metallurgy", edited by K. Mukherjee and J. Mazumder (The Metals Society of AIME, Warrendale, PA, 1981) pp. 1–10.
6. R. K. H. KALIMULLIN and Yu, Ya. KOZHENVNIKOV, *Met. Sci. Heat Treatment* **27** (1985) 272–274.

Received 7 April
and accepted 28 September 1989